

pubs.acs.org/acsapm Article

Control of Drug Release from Microparticles by Tuning Their Crystalline Textures: A Structure—Activity Study

Catherine E. Miles, Ashley D. Bernstein, Thomas M. Osborn Popp, N. Sanjeeva Murthy, Andrew J. Nieuwkoop, and Adam J. Gormley*





ACCESS

Metrics & More

Article Recommendations

Supporting Information

Polymer Pydrophobicity
Polymer Crystallinity
Polymer Themal Properties
Polymer Themal Properties
Drug Release
Drug Release
Time (Days)

ABSTRACT: Predicting drug release profiles from polymer microparticles has proven challenging due to the numerous environmental and chemical factors that affect the device and influence the rate of drug release. By measuring the various polymer properties that can influence drug release, a predictive approach can be used to select polymers with specific properties that will lead to the desired release profile for the application. To illustrate this, a library of tyrosol-derived poly(ester-arylate)s, poly(amide)s, and poly(carbonate)s were used to evaluate the effects of physical (crystallinity, water accessibility, thermal, and hydrophobicity) and chemical (polymer—drug interactions) polymer properties on the release of a highly crystalline drug dexamethasone, which was loaded at a high weight percent (wt %) in microparticles. Nuclear magnetic resonance (NMR) experiments showed that the polymer and drug were not chemically interacting and instead exist as a physical mixture even after exposure to physiological conditions. Polymer crystallinity data revealed that crystallite size was strongly correlated with faster drug release, suggesting that larger crystallites reduce the tortuosity for dexamethasone to diffuse out of the particle matrix. This correlation observed in particles with and without the drug was reproduced with bulk polymers, indicating that crystallinity data from bulk polymers can be used to predict release profiles without having to prepare drug-loaded particles. Consistent with the crystallinity data, particle pore sizes of representative formulations showed that particles with larger pores resulted in faster dexamethasone release. Interestingly, thermal properties (glass transition temperature and melting temperature), polymer hydrophobicity, and molecular weight retention at the end of the 119-day release study did not show any correlation with drug release.

KEYWORDS: controlled drug delivery, polymer structure—property relationships, polymer XRD crystallite size, NMR cryoporometry, microparticles, dexamethasone

■ INTRODUCTION

Delivery of active pharmaceutical ingredients (APIs) requires precise dosage formulations with well-defined release profiles to maintain effective dosage levels while avoiding toxic drug concentration levels. Polymeric drug delivery devices address the problem of high API dosages often required to achieve a drug concentration within the therapeutic range that cannot be achieved with conventional drug administration (tablets, capsules, injections). ^{1,2} In recent years, such polymer—drug delivery devices have flourished, resulting in numerous drug depots, implants, and nanomedicines capable of controlled drug delivery. ^{3,4} Nano- and microparticle drug delivery systems

have been widely successful in controlled release of both hydrophobic and hydrophilic APIs with delivery times of a few hours to several months. 5,6 Microparticles offer advantages over other drug delivery devices due to their ease of processing, convenient administration using standard needles, and the

Received: September 20, 2021 Accepted: November 8, 2021 Published: November 19, 2021





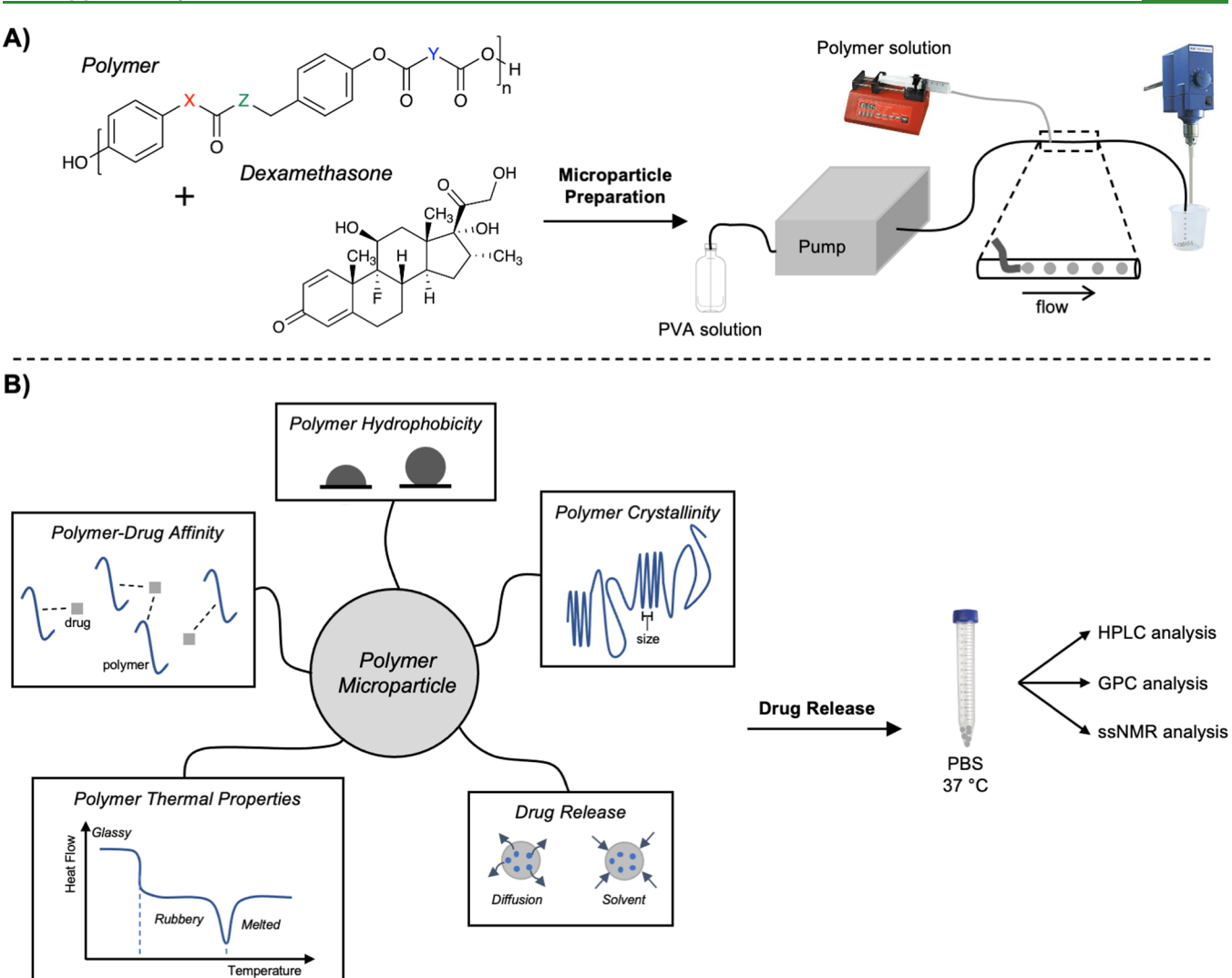


Figure 1. Experimental design schematic. (A) Polymer and drug selection of a series of poly-esters, -amides, and -carbonates with different physical and thermal properties. Microparticle formation was achieved using a continuous flow method to prepare particles ranging from 50 to 180 μ m in diameter. (B) Polymer crystallinity, hydrophobicity, thermal properties, affinity for dexamethasone, and the mechanism of drug release were evaluated and release studies conducted on all formulations to determine which polymer properties affect drug release under *in vitro* conditions.

ability to administer the drug-loaded particles directly to the target site. ^{7,8} These devices are made from synthetic polyesters, -amides, and -carbonates, including commonly used poly(glycolic acid) (PGA), poly(lactic acid) (PLA), and poly(lactic-co-glycolic acid) (PLGA) due to their biodegradable and bioresorbable properties. ^{9–11}

Drug release from a polymer matrix often occurs by diffusion through the polymer matrix or through water-filled pores, polymer swelling, or by erosion of the polymer matrix. 12,13 Mathematical modeling has frequently been used to predict drug release profiles from polymeric devices; however, these models are only accurate at early release timepoints. 14–16 Drug release can be affected by polymer degradation, molecular weight, thermal properties, crystallinity, and its affinity with the drug. 17–20 Predicting drug release from polymer formulations has proven challenging due to interactions between the polymer and the device design and also environmental conditions (pH, osmolality, temperature), which can affect the rate of drug delivery. Substantial research has been carried out to study the effect of device size and shape, surface modifications, and the changes in environmental conditions

such as pH or temperature on drug release rates.^{21–26} While such studies are beneficial for understanding, controlling, and predicting a single polymer matrix, these results cannot be carried over to the case of drug release from multiple polymers. Here we study drug release in many different polymers, and ask the question: which aspects of the polymer's physical and chemical properties most affect drug release?

To answer this question, a large number of polymers consisting of variations from a recently developed tyrosol poly(ester-arylate) library,²⁷ a poly(ester-amide), a poly(ester-arbonate), and two commercial polymers, including PLGA and poly(L-lactic acid) (PLLA), were selected. While the tyrosol-derived polymers are not currently Food and Drug Administration (FDA) approved, they are currently being investigated as alternative polymers for drug delivery, 3D printing applications, and orthopedic devices due to their good resorption, controllable degradation, and less acidic degradation products.^{27–31} Such a polymer library allows us to tune polymer thermal, hydrophobicity, and crystallinity properties without having to dramatically change the polymer chemical structure or mechanical weight. Therefore, a thorough

investigation of the physical and chemical properties of the polymers was carried out to deduce correlations between fundamental polymer properties and the release rate of dexamethasone from microparticles (Figure 1). Dexamethasone was selected as a model API as it has previously been incorporated into PLGA microparticles for controlled release applications.³² Polymer-drug interactions within the microparticles were further studied to determine its impact on the rate of drug release. We found that when polymer-drug interactions are negligible, focus can be on polymer physical properties to predict drug release. It is important to note that here we studied a crystalline drug, which was loaded at a high loading, 20 wt %. Further investigation into if these results are translatable to other drugs and if they are valid when polymerdrug interactions are present are required before these results can be translated to other polymer systems. However, even with these limitations, the results of these studies aim to form a basis for selecting polymers based on their properties to achieve a desired drug release profile so that focus can instead be targeted on designing novel polymers.

MATERIALS AND METHODS

Chemicals and Materials. PLGA-Resomer 506 (50:50 ratio of lactic acid:glycolic acid) and PLLA-Resomer L 206 were purchased from Boehringer Ingelheim. Tyrosol-derived polymers were synthesized as previously described. Paramethasone was provided by Lubrizol Life Science. Water soluble poly(vinyl alcohol) (PVA, molecular weight 30,000–70,000 Da) was purchased from Sigma-Aldrich. Phosphate buffered saline (PBS) solution was prepared using PBS solids (Sigma-Aldrich) at pH 7.4. Sodium dodecyl sulfate (SDS) and sodium azide were purchased from Chem-Impex International Inc. and Sigma-Aldrich, respectively. All solvents were purchased from VWR and Sigma-Aldrich.

Microparticle Preparation. Microparticles were prepared as previously described. ³¹ Briefly, an oil/water (o/w) coaxial flow system was used with a constant flow of PVA solution as the carrier solution (Figure 1A). A syringe pump was used to add the polymer/drug solution at a controlled rate to the PVA carrier tube. Dexamethasone was loaded at 20 weight percent (wt %) attempted loading, as a solid suspension by weighing both polymer and drug along with dichloromethane (DCM) to fully solubilize the polymer. As drug was loaded as a solid suspension, solutions were vortexed to ensure a homogeneous drug distribution. Particles were collected subsurface in a beaker filled with PVA solution (2.5% w/v) fitted with an overhead stirrer. Microparticles were continuously stirred to surface harden the particles through the removal of DCM. After 30 min, the particles were collected, washed with DI water, and lyophilized to dryness. Particles were characterized as described in the following sections.

Particle and Drug Size Analysis. Microparticle size was analyzed from optical images captured using a Nikon 249280 Optiphot-pol microscope with QCapture Suite. A representative image was captured from each particle formulation and between 88 and 504 particles per sample were measured using ImageJ software. Dexamethasone particle size was measured using dynamic light scattering (DLS). Measurements were taken at 25 °C using a class I laser on a Malvern Zetasizer Nano S particle size analyzer. Zetasizer software (version 7.12) was used to measure the particle size by averaging 12 data sets (three samples, four measurements each).

Release Studies. Dexamethasone release medium consisted of PBS + 0.02% w/v sodium azide + 0.05% w/v SDS, where SDS was added to increase the solubility of dexamethasone. Microparticles, ~8 mg, were weighed into 15 mL conical tubes and 14 mL of release medium added to each tube. Tubes were placed on their side with orbital shaking (100 rpm, 0.56 N centrifugal force) in an incubator at 37 °C. At predetermined time points, samples were centrifuged and an aliquot of medium (3–10 mL) was removed and replaced with fresh medium. The removed medium was analyzed using HPLC to

quantify dexamethasone. Sink conditions were maintained by adjusting the volume of medium removed at each time point and known dexamethasone saturation limits. At the end of the study, all medium was removed, samples lyophilized to dryness, and residual particles analyzed by high performance liquid chromatography (HPLC) and gel permeation chromatography (GPC) to determine remaining drug present and polymer molecular weight number $(M_{\rm n})$ retention, respectively.

High-Performance Liquid Chromatography. Drug encapsulation was evaluated by HPLC on the drug extracted from the microparticles. The extraction was performed by first dissolving the microparticles in 15% w/v DCM and 15% w/v dimethyl sulfoxide (DMSO) to dissolve both the polymer and drug, respectively. After 30 min of shaking, 200% w/v methanol (MeOH) was added to precipitate the polymer. After an additional 30 min of shaking, the samples were filtered through a 0.45 μm PTFE filter and run on an Agilent HPLC system (1260 Infinity II) equipped with a Waters (Atlantis T3 C18 150 mm 5 μ m) analytical column. The mobile phase consisted of A, water + 0.05% phosphoric acid (H₃PO₄), and B, acetonitrile (ACN) + 0.05% H₃PO₄, and was run using a gradient starting at 75:25 (A:B), holding for 4 min then transitioning to 50:50 (A:B) over 4 min, then to 90:10 over 4 min, holding for 3 min, then returning to 75:25 (A:B) over 3 min. Samples were run at 35 °C at a flow rate of 1.0 mL/min and detected at a wavelength of 245 nm.

Gel Permeation Chromatography. A Waters GPC equipped with a 717 plus autosampler, 515 HPLC pump, two Agilent PL gel columns in tandem (103 and 105 Å (5 μ m), 30 cm), and a 2489 RI detector was used to analyze $M_{\rm n}$ of bulk polymers and drug and non-drug-loaded microparticles. Samples were prepared in chloroform (CHCl₃) at 2 mg/mL and filtered using a 0.45 μ m polytetrafluoroethylene (PTFE) filter prior to injection. The mobile phase consisted of CHCl₃ + 0.1% trifluoroacetic acid (TFA) and was run at a flow rate of 1 mL/min for 24 min at room temperature.

Differential Scanning Calorimetry (DSC). Thermal transitions were measured using a Mettler Toledo DSC823. \sim 1–2 mg of dried sample was sealed in a 40 μ L aluminum pan. Data were collected using a heat–cool–reheat cycle (–45 to 250 °C, 10 °C/min, 2 min hold time at the starting/ending temperatures). The melting ($T_{\rm m}$) and glass transition ($T_{\rm g}$) temperatures of the samples were determined using the second heat.

Air—Water Contact Angle (AWCA). Samples were prepared by spin coating 12 mm diameter glass coverslip with 100 μ L of polymer solution (2% w/v polymer in DCM). Coverslips were spun at 3000 rpm (120 N centrifugal force) for 30 s followed by drying for 24 h under vacuum at 40 °C to facilitate the removal of residual solvent. A Ramé-Hart Model 100–00 goniometer was used to measure AWCA following ASTM C813. A single drop of ultrapure water (7 μ L) was added to the polymer surface and the angle of the droplet measured. All measurements were performed in triplicate (three drops/coverslip on three separate coverslip).

Solubility Parameters for the Prediction of Polymer–Drug Miscibility. The Hildebrand solubility parameter, δ , was calculated using the Hansen solubility parameter (HSP), which was calculated from the individual group contribution of each functional or structural group. ^{34,35} The Hoftyzer–van Krevelen method (HVK) was used for the individual partial solubility parameters, $F_{\rm div}$ $F_{\rm piv}$ and $E_{\rm hiv}$ and molar volume (ν_i), which were taken from the literature. ³⁶ Group-specific ν_i values and the total $V_{\rm m}$ value were calculated by Fedor's method using the individual ν_i values obtained from the literature. ³⁶ PLGA, PLLA, dexamethasone, and water $\delta_{\rm T}$, $\delta_{\rm D}$, $\delta_{\rm P}$, $\delta_{\rm Hv}$ and $V_{\rm m}$ values were also taken from the literature. ^{37–39} Values for the partial and total solubility parameters $\delta_{\rm D}$, $\delta_{\rm P}$, $\delta_{\rm Hv}$ and $\delta_{\rm T}$ and molar volume, $V_{\rm m}$ are shown in Table S1.

The drug-solvent or drug-polymer compatibility was estimated using the Flory-Huggins interaction parameter (χ):

$$\chi_{\text{polymer-drug}} = (\delta_{\text{T,polymer}} - \delta_{\text{T,drug}})^2 \times \frac{V_{\text{m,drug}}}{RT}$$
(1)

Figure 2. Chemical structures of (A) tyrosol-derived poly(ester-arylate)s with varying carbon chain and functional groups; and (B) poly(ester-amide), poly(ester-carbonate), and PLGA and PLLA control polymers selected for drug loading and release studies.

Table 1. Properties of Tyrosol-Derived Polymers and PLGA and PLLA Control Polymers and Model Drug Dexamethasone Selected for Drug Loading and Release Studies

substrate	abbreviation	$M_{\rm n}$ (kDa) ^a	AWCA (degrees) ^b	v	$log P^d$	$({}^{T_{g}}({}^{g})^{e})$	$T_{\rm m}$ (°C) e	$(^{\circ}C)^{e}$
		(KDa)	(degrees)	X substrate-water				(C)
dexamethasone	DEX		()	3.03	1.83	117	265 ⁴⁸	
poly(HTy glutarate) ester	pHTy3	50	73.5 (0.8)	4.22	3.63	31	137 (127)	85
poly(DTy glutarate) ester	pDTy3	101	71.0 (0.8)	4.37	4.08	29	157 (134)	118
poly(HTy adipate) ester	pHTy4	84	72.2 (0.4)	4.37	4.08	22		
poly(DTy adipate) ester	pDTy4	76	68.4 (0.9)	4.51	4.52	23	183	160
poly(HTy suberate) ester	pHTy6	96	74.1 (0.2)	4.63	4.97	8	70	
poly(DTy suberate) ester	pDTy6	95	70.8 (0.7)	4.74	5.41	20	149	126
poly(HTy azelate) ester	pHTy7	69	80.2 (0.5)	4.74	5.41	4	71	
poly(DTy azelate) ester	pDTy7	72	78.7 (0.5)	4.84	5.86	11	118	93
poly(HTy sebecate) ester	pHTy8	139	74.8 (0.4)	4.84	5.87	3	79 (89)	51
poly(DTy sebecate) ester	pDTy8	90	74.7 (0.7)	4.93	6.30	9	150	129
poly(HTy dodecanedioate) ester	pHTy10	99	76.2 (0.5)	5.02	6.75	6	88 (99)	66
poly(DTy dodecanedioate) ester	pDTy10	77	77.2 (0.8)	5.10	7.19	6	153	131
poly(HTy transhexenedioate) ester	pHTyTh	51	73.8 (0.9)	3.97	3.72	35		
poly(DTy transhexenedioate) ester	pDTyTh	48	72.0 (0.3)	4.15	4.16	34	141	116
poly(DTy diglycolate) ester	pDTyDg	44	67.7 (0.1)	4.08	3.11	52	167 (156)	136
poly(HTy cyclohexanedioate) ester	pHTyCh	107	70.0 (0.7)	4.22	4.70	67		
poly(DTy cyclohexanedioate) ester	pDTyCh	117	75.1 (0.8)	3.71	5.10	62		
poly(HTy phenylenediacetate) ester	pHTyPd	69	75.3 (0.5)	4.08	4.84	53	131 (147)	98
poly(DTy phenylenediacetate) ester	pDTyPd	81	74.0 (0.4)	4.22	5.28	47	158	94
poly(desaminotyrosyl-tyrosine dodecyl dodecanedioate) ester	pDTD10	62	88.9 (0.7)	5.51	11.18		59	32
poly(tyrosol diaryl dodecanedioate) carbonate	pTyDi10	95	79.4 (0.8)	4.97	7.51	-2	120	83
poly(lactic-co-glycolic acid)	PLGA	91	65.5 (0.8)	3.71	0.80	48		
poly(L-lactic acid)	PLLA	88	68.5 (0.7)	4.36	1.90	55	175	

 a Values were measured relative to polystyrene standards on CHCl $_3$ GPC. b AWCA values were measured on polymer spin coated coverslips, all measurements were recorded in triplicate with SD shown in parenthesis. c Substrate—water miscibility was calculated according to HVK group contribution theory. d Polymer log p values were calculated using MarvinView software and were calculated considering only a single monomer repeat unit. c Values were measured using DSC, and the T_g and T_m measurements were taken from the second heat. Melting temperatures in parenthesis represent a second, minor melting temperature of the polymer. Melting temperature of dexamethasone was reported from the literature. 48

where R represents the gas constant and T represents the temperature (in Kelvin).⁴⁰ A polymer degree of polymerization (DP) of 1 was used for all calculations.

Calculations of Polymer log*P*. Polymer log*P* values were calculated using MarvinView software (ChemAxon Ltd.). Calculations were based on a single monomer repeat unit without consideration of end group functionality. The log*P* predictor plugin was used to determine individual polymer log*P* values.

X-Ray Diffraction (XRD). XRD data were collected using a Philips Xpert diffractometer in the parafocus geometry with Cu K α radiation. A zero-background holder (single crystal of silicon; (100) plane cut 9° toward (001)) was used with a small amount of silicone grease to hold the samples in place. Scans were obtained from 5 to 55° 2 θ , with 8.0 s per 0.05° step, and no-spin. Polymer percent crystallinity and crystallite size were calculated by subtracting the drug spectrum from the drug-loaded particle spectrum. The grease background was

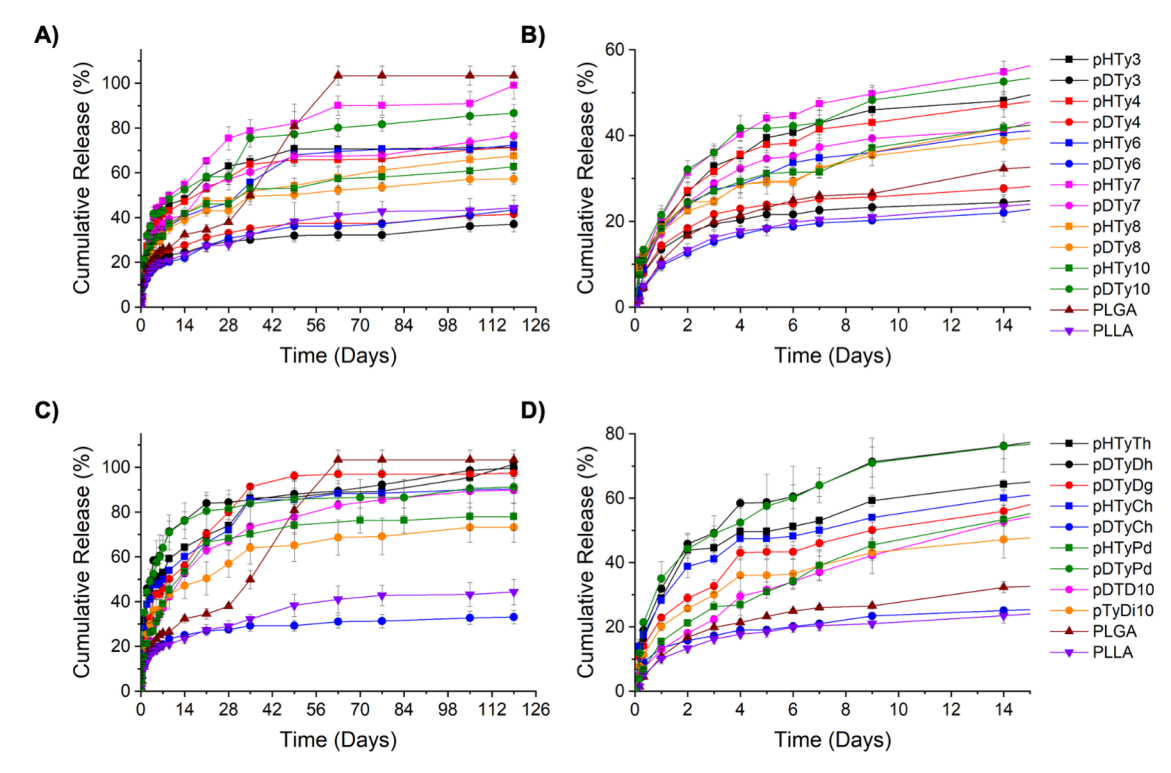


Figure 3. Dexamethasone release profiles of (A) the entire 119-day study and (B) the initial 14 days of different diacid aliphatic carbon chain length microparticles and release profiles of (C) the entire 119-day study and (D) the initial 14 days of different diacid functional group microparticles. All formulations were prepared by loading drug as a solid suspension at 20 wt % attempted loading. Samples were run in triplicate and error bars represent the SD between the three samples removed at every time point.

measured separately and was removed prior to analysis. The polymer peaks between 8 and 40° were profile-fitted with JADE software (Materials Data Inc., CA) using Pearson VII functions (exponential factor = 5, Lorentzian = 0, and skew = 0).⁴¹ Polymer crystallinity and crystallite size were calculated as described in the SI.

Nuclear Magnetic Resonance (NMR) Cryoporometry. Cryoporometry data were acquired for both pDTy4 and pHTy7 on a Bruker Avance III HD spectrometer equipped with an HCN Bruker probe with a lock channel, with a ¹H Larmor frequency of 600 MHz. Polymer particles were added to 5 mm NMR tubes, and ultrapure water added until it just covered the particles and then allowed to soak for at least 24 h before data collection. pDTy4 (22.2 mg) and pHTy7 (17.1 mg) were used with 41.6 and 67.2 mg of water, respectively. Immediately prior to insertion into the spectrometer, the sample was immersed in liquid nitrogen for 5 min. ¹H 1D were acquired at 252.4 to 274.2 K in 0.2 K increments with a 10 min equilibration time at each temperature. All ¹H 1D spectra were processed using TopSpin (version 3.6.1). Microsoft Excel (version 16.16.27) and MatLab (version R2019a) were used to process and analyze the data.

Scanning Electron Microscopy (SEM). Particle morphology was evaluated using a Phenom ProX SEM (Nanoscience Instruments, Phoenix, AZ). Microparticles were deposited onto a double-sided adhesive carbon tape on an aluminum stud. An acceleration potential of 10 kV was used for imaging.

Solid State Nuclear Magnetic Resonance (ssNMR). ssNMR studies of two of the polymer particle formulations (pDTy4 and pHTy7) with and without drug loading, as well as dexamethasone, were acquired on a Bruker Avance III HD spectrometer equipped with an HXY 1.6 mm Phoenix probe with lock tuned to HCN, FC, and HC, with a frequency of 599.7 MHz for 14 H, 150.8 MHz for 13 C, and 564.2 MHz for 19 F. Spectra were acquired at 20 $^{\circ}$ C and at either 20 or 30 kHz magic-angle spinning (MAS). A 90 $^{\circ}$ pulse length of 1.6 μ s was used for 14 H, 2.1 μ s for 13 C, and 2.3 μ s for 19 F. 14 H 1D spectra were acquired with 2 scans and a recycle delay of 8.0 s. 13 C cross polarization (CP) experiments were acquired with 8192 scans, a

recycle delay of 8.0 s, and 2 ms contact time. 19 F 1D spectra were acquired with 4 scans and a recycle delay of five times T_1 .

For all samples, $^{13}\mathrm{C}$ and $^{1}\mathrm{H}$ chemical shifts were referenced to adamantane ($^{13}\mathrm{C}$ downfield peak 38.48 ppm, $^{1}\mathrm{H}$ CH $_{2}$ resonance 1.74 ppm). 42 $^{19}\mathrm{F}$ was referenced to neat dexamethasone. The magic angle was set with KBr by maximizing the intensity of the first-order spinning sideband of the $^{79}\mathrm{Br}$ resonance. 43 1D spectra were processed using TopSpin (version 3.6.1). T $_{1}$ relaxation data were processed using TopSpin (version 3.6.1) and MatLab (version R2019a).

Statistical Analysis. Origin 18.0 software was used for statistical analyses. To compare the variation in drug encapsulation and the residual M_n retention post 119 days of incubation, one-way analysis of variance (ANOVA) and a Tukey multiple comparison post-test were used with significance set at p < 0.05. Results are expressed as mean \pm standard deviation (SD).

■ RESULTS AND DISCUSSION

Polymer and Drug Selection. A series of tyrosol-derived poly-esters, -amides, and -carbonates were selected because of their different physical and thermal properties. PLGA and PLLA were selected as control polymers because of their wide use in biomaterial and microparticle drug delivery applications. 44-46 Dexamethasone, a hydrophobic corticosteroid known for its anti-inflammatory and immunosuppressant effects for the treatment of asthma and neuroinflammation, was selected as a model drug to test drug loading and release from polymeric microparticles.⁴⁷ Dexamethasone and polymer chemical structures are shown in Figures 1A and 2, respectively. Drug and polymer abbreviations, physical, and thermal properties are shown in Table 1. DSC scans of all polymers with varying aliphatic diacid length or diacid functional group, and dexamethasone are shown in Figures S1, S2, and S3A, respectively.

The majority of polymers tested consisted of the tyrosol based polymer (Figure 2A), where X is the carbon atoms in the tyrosol monomer (one or two), and Y is the carbon atoms in the diacid monomer (3–10 or a functional group). When X is one carbon, the monomer is denoted as 4-hydroxyphenethyl 2-(4-hydroxyphenyl)acetate (HTy) and when X is two carbons, 4-hydroxyphenethyl 3-(4-hydroxyphenyl)propanoate (DTy). Poly(desaminotyrosyl-tyrosine dodecyl dodecanedioate) ester (pDTD10) and poly(tyrosol diaryl dodecanedioate) carbonate (pTyDi10) were selected to test how the presence of an amide or carbonate bond impacts drug loading and release (Figure 2B). Additionally, the pH of HTy and DTy at saturation was measured and was >7, indicating that these monomers will not cause a localized acidic microenvironment upon degradation making these monomers ideal for biomaterial applications.

The $M_{\rm n}$ value of the polymers ranged from 44 to 139 kDa. $M_{\rm n}$ has previously been shown to be a property that impacts the rate of drug release and an important parameter for predicting drug release rates; however, at the higher polymer molecular weights used here, the influence of $M_{\rm n}$ is minimal. The percentage of $M_{\rm n}$ retention at the end of the release study was monitored to evaluate the rate of degradation to determine if the difference in starting $M_{\rm n}$ impacted the rate of drug release.

Polymer crystallinity ranged from amorphous to semicrystalline states with both amorphous and crystalline polymers included in this study. Their $T_{\rm g}$ values were both above and below physiological temperature (37 °C). For all polymers with a melting point, the $T_{\rm m}$ was above 37 °C, which is important to ensure that the polymers were not undergoing a thermal phase transition during the release study. The AWCA, $\chi_{\rm polymer-water}$, and $\log P$ (a measure of substrate solubility in an organic vs an aqueous solvent) are useful parameters in understanding the hydrophobic nature of the polymer. Increasing the diacid chain length resulted in an increase in polymer hydrophobicity and HTy polymers had a lower calculated $\chi_{\rm polymer-water}$ and $\log P$ than their corresponding DTy polymers.

Drug Loading and Release from Polymeric Microparticles. The o/w continuous flow method (Figure 1A) was successfully used to prepare particles ranging from 50 to 180 μ m in diameter (Figure S4). The small size range of these microparticles allows them to be used as an injectable drug delivery system or implanted during an operation. This optimized continuous flow method eliminates the harsh stirring conditions often observed in emulsification techniques, and after drying, prepared particles appeared free flowing. Micronized dexamethasone (965 nm \pm 192) was used for drug loading (Figure S3B). Drug loading capacity (LC) was calculated using eq 2, and a high LC (>16 wt %) was achieved for all formulations.

$$LC\% = \frac{\text{total drug encapsulated}}{\text{total microparticle weight}} \times 100$$
 (2)

The release of dexamethasone from microparticles of each of the polymers was studied at 37 °C for 119 days. Differences in dexamethasone release rates can be seen in the release profiles shown in Figure 3. Commercially available PLGA showed the fastest release, exhibiting a commonly observed second burst release at 28 days caused by polymer degradation, which often occurs between 25 and 35 days under physiological conditions. S4,55 Only pHTyTh, pDTyTh, and pHTy7 poly-

mers released all dexamethasone by the end of the 119 days. pDTyCh had the slowest release of all formulations, releasing only 33% after 119 days. The poly(ester-carbonate) and poly(ester-amide) polymers released 90 and 73% dexamethasone, respectively, after 119 days.

The release of dexamethasone was faster in HTy polymers than from their respective DTy polymers when the diacid consisted of an aliphatic carbon chain, with the exception of the longest aliphatic chain length (pDTy10). Additionally, for the DTy polymers, increasing the diacid aliphatic chain length resulted in faster dexamethasone release; however, the same trend did not translate to the HTy polymers (Figure 3A). Interestingly, when a functional group (Th, Cd, Dg, Pd) was incorporated as the diacid, the release rate was faster in HTy polymers than in their respective DTy polymers, with the exception of pDTyPd. The Th monomer resulted in the fastest dexamethasone release out of the functional diacids for both the HTy and DTy polymers. The same trend did not hold true for any other polymer pair, in fact the Ch polymers showed the largest difference in dexamethasone release between the HTy and DTy polymer pair (56%). Comparing the Th formulations to their corresponding four carbon chain diacid, the Th polymers resulted in faster drug release, which could be due to either the increased polymer hydrophilicity (logP and $\chi_{\text{substrate-water}})$ or the increased polymer rigidity. Only PLGA showed a second burst release, while all tyrosol-derived polymers showed biphasic release. At the end of the study, all formulations except for PLGA were digested for HPLC analysis and all formulations except for pHTyTh, pDTyTh, and pHTy7 contained residual dexamethasone. Particle size was not the only parameter controlling dexamethasone release as no clear correlation between cumulative release and particle size was observed for these formulations (Table S3).

Analysis of the release profiles from the different formulations show that the primary factors governing dexamethasone release for a given polymer could be the polymer's physical properties and the interactions between dexamethasone and the polymer. It is possible to understand which properties are affecting drug release trends by analyzing the polymers' crystallinity, water accessibility, thermal, hydrophobicity, and affinity for dexamethasone.

Polymer Physical Properties. Polymer Thermal Properties. $T_{\rm g}$ and $T_{\rm m}$ values of bulk polymers, empty particles, and drug-loaded particles are compared with LC in Table S2. The $T_{\rm g}$ values are similar in bulk and empty particles but increase with drug loading due to the incorporation of dexamethasone that has a high $T_{\rm g}$ (117 °C). The observed increase in $T_{\rm g}$ of the drug-loaded particles was expected with incorporating a high $T_{\rm g}$ drug. A single $T_{\rm g}$ value was observed during the second heat, indicating polymer—drug miscibility for all formulations prepared after temperature processing. The incorporation of drug either decreased or caused a complete disappearance of $T_{\rm m}$. This suggests that dexamethasone reduces the polymer crystallinity in the particle like an impurity would.

To determine the effect of the thermal properties on drug release, three representative release time points that correspond to the three phases of drug release were selected: (i) the initial burst release period at day 7, (ii) the beginning of the sustained release period at day 21, and (iii) the end of the release study at day 119. Cumulative percent drug release at each of these time points was compared against the polymer thermal properties in the form of matrix plots. Pearson's r and linear fits were used to draw correlations between the two

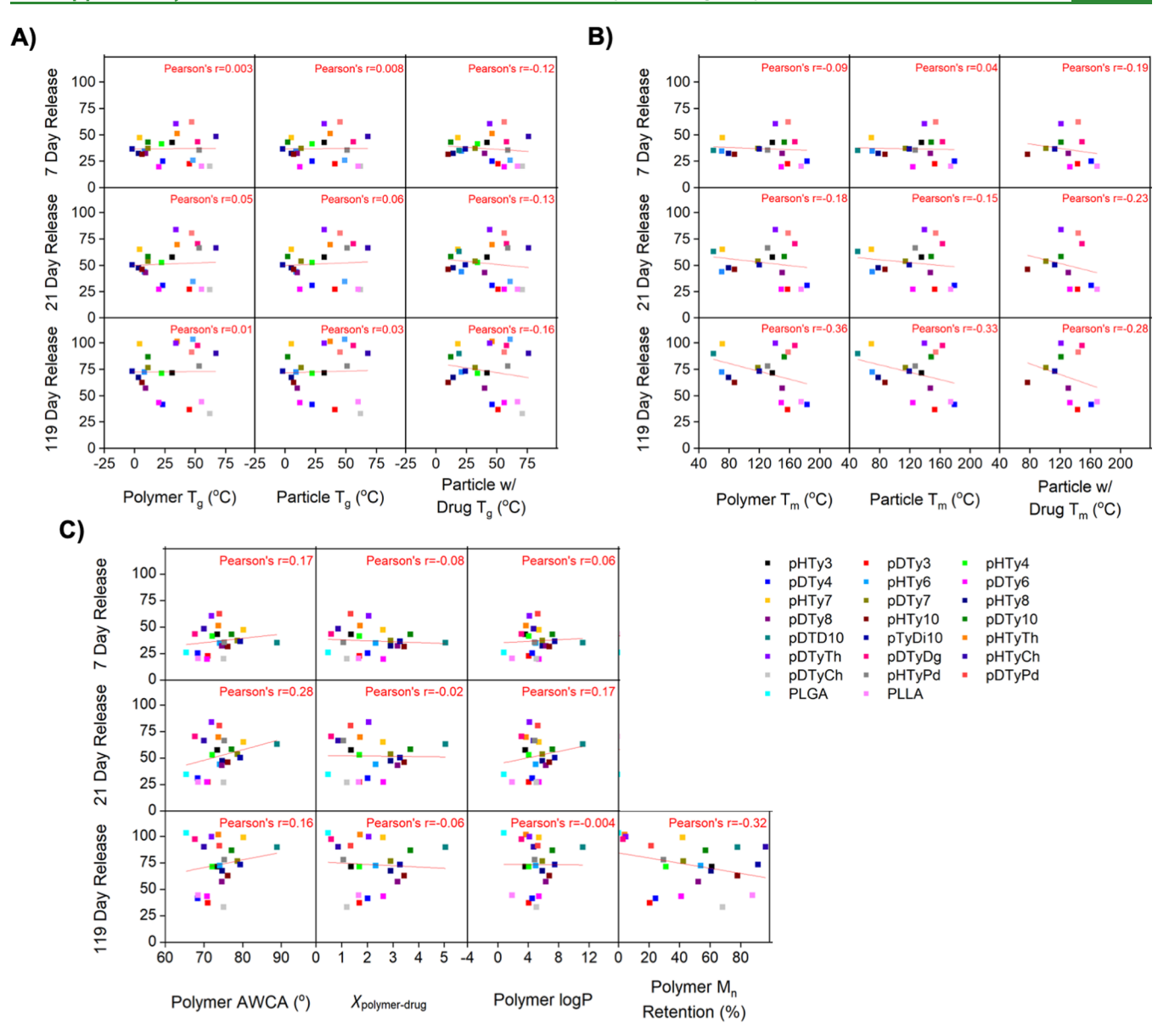


Figure 4. Matrix plots comparing cumulative dexamethasone release at 7, 21, and 119 days to (A) $T_{\rm g}$ of bulk polymer, particle, and particle with drug; (B) $T_{\rm m}$ of bulk polymer, particle, and particle with drug; (C) bulk polymer AWCA, $\chi_{\rm polymer-drug}$, logP, and polymer % $M_{\rm n}$ retention after 119 days exposure to physiological conditions.

independent variables. It was hypothesized that if the $T_{\rm g}$ of the polymer was below physiological temperature (37 °C), the polymer would be in a rubbery state and dexamethasone release would be faster compared to polymers with a $T_{\rm g}$ value above 37 °C, which would be in a glassy state. A polymer in a rubbery state has higher chain mobility, which facilitates water penetration and enhances drug diffusion rates. ⁵⁷ But, little correlation between $T_{\rm g}$ ($r \sim 0.1$) or $T_{\rm m}$ ($r \sim 0.2$) and the drug release rates are shown by the linear fits and corresponding Pearson's r values.

Polymer Hydrophobicity and Degradation. Polymer hydrophobic properties (AWCA and $\log P$) of the bulk polymers were compared to drug release and no correlation was observed between cumulative drug release at 7, 21, and 119 days with either property (Figure 4C). GPC retention of digested particles showed a wide range in $M_{\rm n}$ retention after exposure to release medium at 37 °C for 119 days (Figure SS). No PLGA particles were present at the end of the 119-day

study indicating that complete degradation and resorption occurred. The starting polymer $M_{\rm n}$ does not appear to be the sole contributor impacting drug release as no clear trend between the highest polymer $M_{\rm n}$ and % drug release after 119 days was observed (Table S3). There is a slight correlation with % $M_{\rm n}$ retention as seen in the matrix plot in Figure 4C ($r \sim 0.3$); however, this correlation is due to the handful of formulations, which retained very little $M_{\rm n}$ (0–5%) no longer maintaining their polymeric matrix, which is needed to hold the drug inside of the particle.

Polymer Crystallinity and Crystallite Size. A subset of polymers, including fast and slow releasing formulations, HTy and DTy monomers, and aliphatic carbon and functional group diacid monomers were analyzed by XRD. Bulk polymer, empty particles, and drug-loaded particles of each polymer selected were analyzed to understand how particle formulation and the presence of drug affects polymer crystallinity (Figure 5). The sharp peaks present in the drug-loaded particle spectra

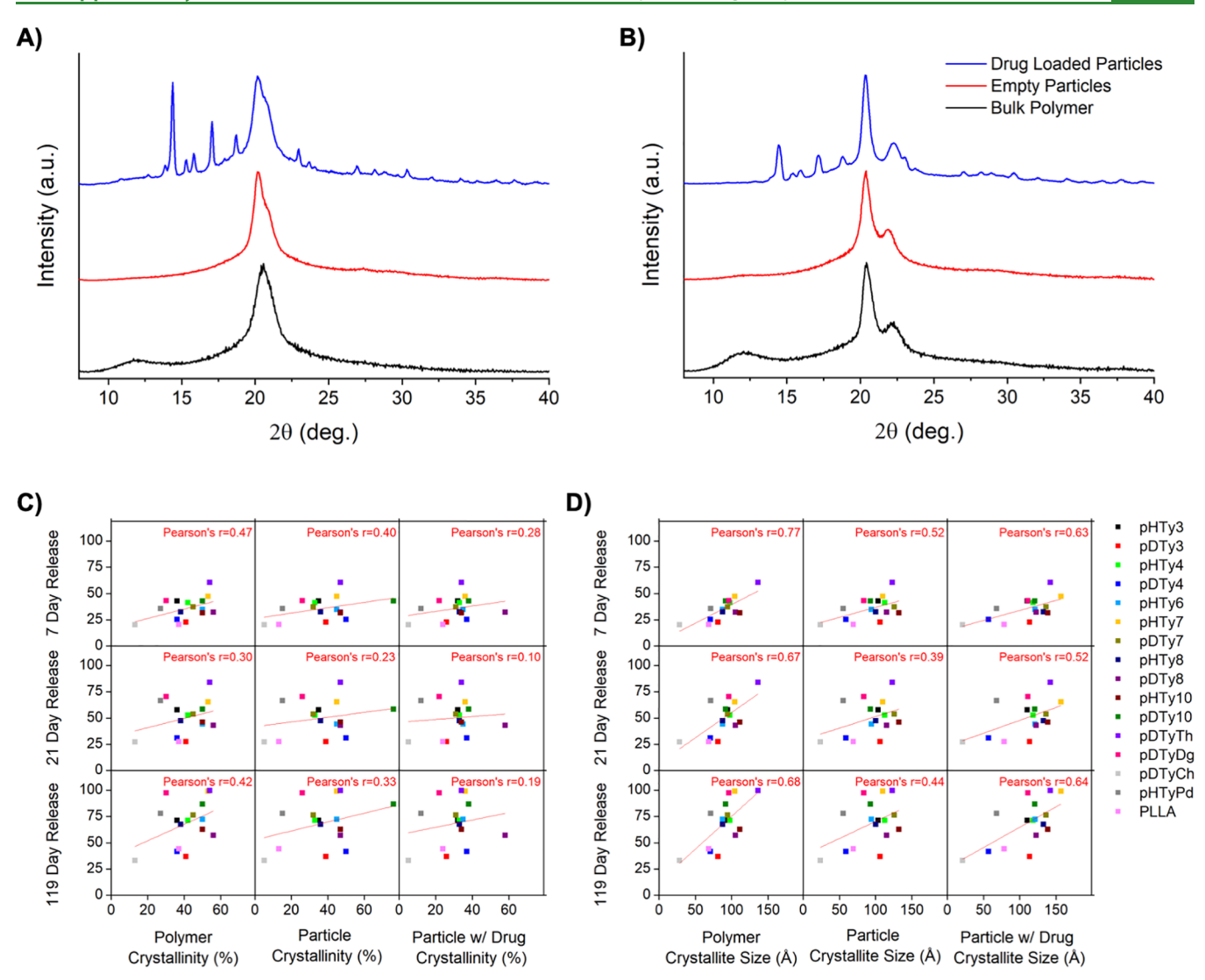


Figure 5. XRD analysis of (A) pDTy4 and (B) pHTy7 bulk polymer, empty particles, and dexamethasone loaded particles prepared at 20 wt % attempted drug loading. Scans have been offset for clarity. Matrix plots comparing cumulative dexamethasone release at 7, 21, and 119 days to bulk polymer, empty particles, and drug-loaded particles (C) polymer % crystallinity and (D) polymer representative crystallite size.

are due to dexamethasone, which remains in its crystalline state after particle formulation. Interestingly, dexamethasone appears to be more crystalline in pHTy7 particles than in pDTy4 particles; this is consistent with ¹⁹F NMR T₁ relaxation data shown in Table S4. For comparison, an XRD scan of dexamethasone is shown in Figure S6. Polymer crystallinity and crystallite size were calculated from profile-fitted scans (Table S6). The crystallite size was calculated from the most representative of the polymer peaks using the Scherrer equation. The details of these calculations are described in the SI and an example spectrum are shown in Figure S7. All the polymers run on XRD were semi-crystalline, although pHTyPd, pDTyCh, and PLLA were less crystalline than others. For all polymers except for pDTy4 and pDTy10, the polymer percent crystallinity decreased upon particle formulation. Thereafter, the crystallinity either remained constant or decreased with drug incorporation, except in the case of PLLA and pDTy8 where drug incorporation increased the polymer crystallinity.

To determine the effect of the polymer crystallinity on drug release, cumulative percent drug release at the same three time points (7, 21, and 119 days) was compared against the polymer properties in the form of matrix plots. Drug release is expected to be affected in some way by the structure and morphology of the polymer matrix within which the drug is embedded. Therefore, this aspect was explored by using characteristics of the structure seen in the XRD data. Since drug molecules are mostly segregated in the amorphous regions of a polymer, which are more permeable and accessible to water, it is generally assumed that drug release rate is higher in polymers with higher amorphous content, i.e., with lower crystallinity. 17,19,58 Our data also show a trend opposite to that commonly assumed. The matrix plot in Figure 5A shows a weak correlation at all three time points for bulk polymer crystallinity, indicating that polymers with higher crystallinity have a faster release rate ($r \sim 0.4$). This suggests that there are other factors that confound this simple correlation between the crystallinity and drug release. For instance, in one study, higher drug release rates were observed in microparticles with higher crystallinities.⁵⁹ This trend was attributed to crystalline morphology causing rougher surface texture on the microparticles, which in turn caused rapid drug release. We found that there is a significantly stronger correlation between another measure of crystalline order, the crystallite size ($r \sim$

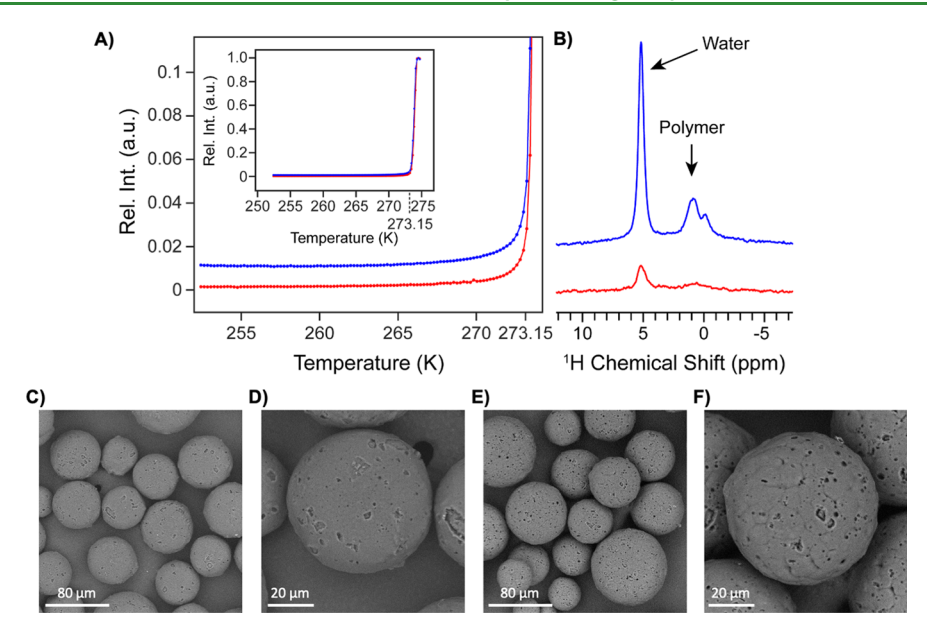


Figure 6. NMR Cryoporometry results. (A) Melting curves of water within pDTy4 (blue) and pHTy7 (red) particles approaching the bulk melting point (273.15 °C) and full melting curve (inset) prepared by plotting temperature vs the relative integration of the water peak. (B) ¹H 1D NMR spectra of pDTy4 (blue) and pHTy7 (red) at 252.4 K, normalized to the amount of bulk water present in each sample. Representative SEM images of pDTy4 (C and D) and pHTy7 (E and F) particles at 1000× (80 μm scale bar) 3000× (20 μm scale bar) magnification.

0.7; Figure 5B), suggesting that a larger crystallite size leads to faster drug release. This correlation can be found in the microparticles without drug and in microparticles with drug as early as the 7-day time point, and the trend held out to 119 days.

In a detailed study, Jeong et al. found that the correlation between increased drug release rates in polymer and lower crystallinity is not robust, and an opposite trend can be discerned in some subclasses of samples. 19 Perhaps in acknowledgment of this uncertainty, they attributed faster release not to a higher crystallinity, but to the coarse microstructure of the particles. Our observation of larger crystallite size is a confirmation of this hypothesis. Our data suggest that the microstructure can be quantified in terms of crystallite size. Other parameters such as degree of crystallinity and porosity are known to affect the drug release rate; crystallinity by defining the amorphous volume available for drug incorporation and migration, and the porosity that provides a local microenvironment for the drug to be solubilized in the medium that diffuses into the pores and be transported out of the matrix. Smaller crystallites will increase the path length for the diffusion of the drug molecules by increasing the tortuosity, and thereby contribute to slower drug release. Note that in Figure 5D, the correlation between drug release and crystallite size is highest at the 7-day time points, and lowest at the 119-day time point. This suggests that once the pathways between the crystallites are filled, the influence of crystallite size on drug release is diminished. This further validates our hypothesis that crystallite size plays a role in determining the rate of drug release.

Particle Porosity. As the structure of the polymer network is strongly correlated with drug release, we sought to better understand the nature of the pore environment in these polymers. NMR cryoporometry is a technique in which the NMR signal of a pure liquid saturating a porous sample is monitored as a function of temperature. As liquids confined within pores exhibit a melting point depression by the Gibbs—

Thomson effect, this method takes advantage of the change in NMR signal linewidth between solid and liquid to observe the temperature at which the confined liquid undergoes the phase transition. The Gibbs—Thomson equation describes the relationship between the melting point depression of water $(\Delta T_{\rm m})$ in a porous material and its pore diameter (d), and can be represented in a simplified form as shown in eq 3:

$$\Delta T_{\rm m} = T_{\rm B} - T_{\rm m}(d) = \frac{k_{\rm GT}}{d} \tag{3}$$

where $k_{\rm GT}$ is a constant that depends on the properties of the liquid, the pore geometry, and the interfacial surface energy between the liquid and the pore walls. When the signal area is plotted against temperature, a sharp step may be observed at the melting point of the confined liquid for systems with a monodisperse pore size distribution. However, for pore networks with complex geometries and a broad distribution of pore diameters, step-like changes in the signal with temperature may not necessarily be observed. 62

The polymers pDTy4 and pHTy7 were examined with NMR cryoporometry using water as the confined liquid. A benefit of using water for the analysis is that we are directly probing the water-accessible pore volume, which is the pore volume relevant to the kinetics of drug release. Neither of the polymers show noticeable steps in their melting curves (Figure 6A), indicating that both the pDTy4 and pHTy7 pore networks consist of a broad distribution of pore diameters.

Below the bulk melting point of water, a liquid water signal persists within the pores of pDTy4 even at a temperature of 252.4 K, while at this temperature within pHTy7, a much smaller amount of water signal remains (0.1%). Figure 6B shows a significantly more intense water peak for pDTy4 than for pHTy7 at 252.4 K. There are mobile polymer resonances still visible in Figure 6B, but they were not part of the integration for the data shown in Figure 6A. Values of $k_{\rm GT}$ for pDTy4 and pHTy7 polymers were calculated to be 84 nm K and 91 nm K, respectively. Calculation details are described in

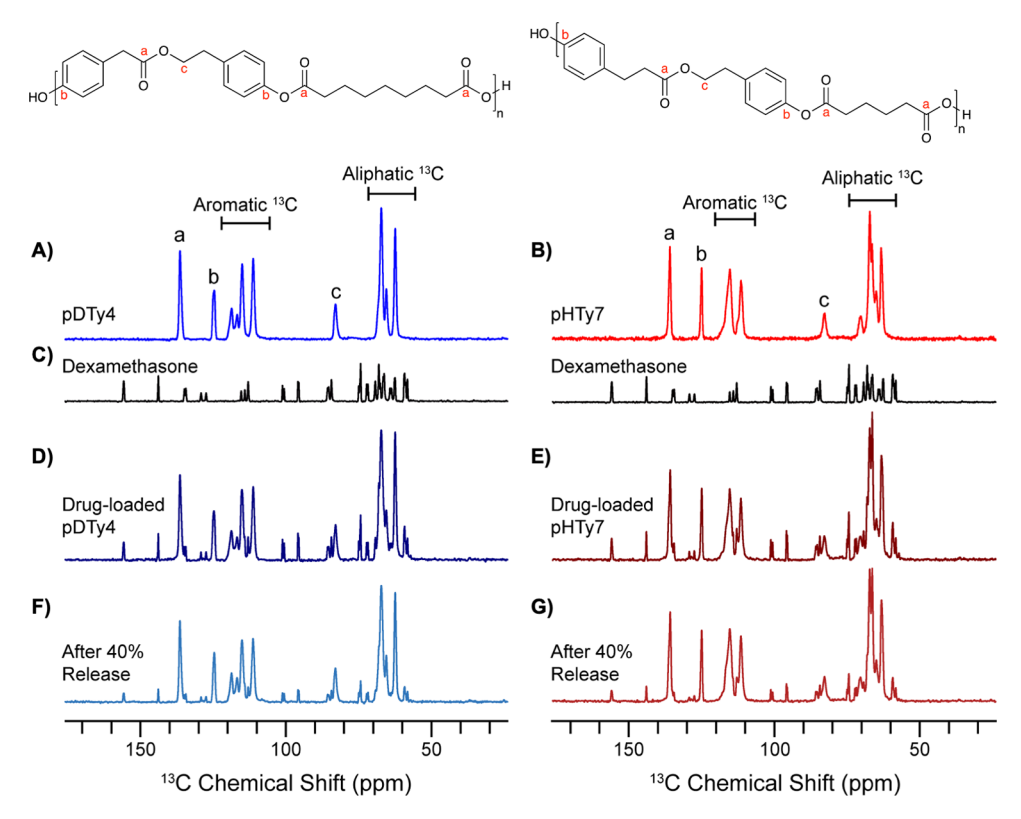


Figure 7. CP-MAS ¹³C ssNMR of (A) pDTy4 particles, (B) pHTy7 particles, (C) dexamethasone, (D) pDTy4 dexamethasone loaded particles, (E) pHTy7 dexamethasone loaded particles, (F) pDTy4 dexamethasone loaded particles after ~40% drug release, and (G) pHTy7 dexamethasone loaded particles after ~40% drug release. Assignments of the polymer peaks are shown, and spectra have been offset for clarity.

the SI. Utilizing these values as inputs for eq 3, we find that a melting temperature of 252.4 K corresponds to a pore diameter of approximately 4 nm for both polymers, and that a melting temperature of 270 K corresponds to a pore diameter of 27 nm for pDTy4 and 30 nm for pHTy7. As a negligible amount of water remains liquid below 270 K within pHTy7, the majority of the pore volume of pHTy7 is comprised of pores with a minimum diameter of 30 nm. However, for pDTy4, 1.1% of the total water volume remains unfrozen even at the lowest measured temperature of 252.4 K, meaning that of the total water-accessible pore volume in pDTy4, 23 μ L/g of this volume is comprised of channels 4 nm or less in width. As water was able to enter these pores during the cryoporometry experiments, this indicates that they serve as functional pores for drug release. This difference in the pore size distribution for pDTy4 and pHTy7 can be related to their release profiles, as the smaller diameter and more tortuous network of pores within pDTy4 results in slower dexamethasone release than for pHTy7.

These results complement the SEM images shown in Figure 6C–F, which highlight the morphological features of the particles. Visually, pHTy7 particles have larger surface macropores that are more abundant compared to pDTy4 particles. After drug release, particle porosity did not visually appear to change as seen in the SEM images taken after 119 days at 37 °C, suggesting that the polymer retains its matrix form and is able to retain dexamethasone inside of the particle (Figure S8). The overall pore network of the pHTy7 particles is such that larger macropores lead into larger nanopores (greater than 30 nm) present inside of the polymer matrix. This is consistent with the larger crystallite size from XRD experiments, confirming that the particle matrix is more loosely

packed. For pDTy4 particles, there are fewer surface macropores present and as revealed from cryoporometry data, at least 1.1% of the micropore volume is 4 nm or less in diamter. These smaller micropores connect to the rest of the pore network to make up the inside of the particles. This is again consistent with XRD data, which showed a smaller crystallite size resulting in a more tightly packed particle matrix

Dexamethasone Release Mechanisms. Release kinetics were analyzed by fitting the release profiles using zero-order, first-order, and Higuchi models to predict the drug release mechanisms. 63-65 For all formulations, the Higuchi model resulted in the highest correlation coefficient (r^2) as shown in Table S6, indicating that diffusion-based drug release occurred in all formulations. Thus, as water penetrates into the matrix, dexamethasone is dissolved and diffuses out of the particle. According to the Korsmeyer-Peppas model, which predicts the diffusion mechanism, n < 0.5 is considered Fickian diffusion while 0.5 < n < 1 is non-Fickian (anomalous) diffusion, where n is the release exponent derived from the Korsmeyer–Peppas equation. 66,67 Calculated *n* values are shown in Table S6. Release profiles modeled with the Korsmeyer-Peppas equation (Figure S9) show that pDTD10, pHTyPd, and PLGA formulations show anomalous diffusion, which indicates that a polymer or environmental parameter is impacting drug release. All other formulations show Fickian diffusion where drug solubility and water accessibility control the rate of drug release.

Applying fitting models such as the Higuchi and Korsmeyer–Peppas models requires several assumptions including that the diffusivity of the drug is constant and unidirectional. This assumes that our spherical particles

have homogeneous and uniform size porosity. As demonstrated previously in the cryoporometry calculations, pDTy4 and pHTy7 particles have non spherical and varying size pores. These differences in porosity can contribute to the anomalous diffusion calculations derived from the kinetic models. These fitting mechanisms are accurate only up to 60% cumulative drug release after which the fitting profiles deviate from experimental results.

Polymer Chemical Interactions. Polymer—Drug Miscibility. The miscibility of the polymers and dexamethasone are shown in Table S7. Increasing the diacid chain length decreased the miscibility of the polymer and dexamethasone; however, HTyCh, DTyDg, and PLGA values were <1.0 indicating some polymer—drug miscibility. The miscibility parameter is likely not influencing drug loading since the particles were prepared using a solid drug suspension. The miscibility parameter has been previously used in predicting drug loading when both the polymer and drug were fully solubilized during particle formation. Matrix plots did not show a correlation between cumulative release at 7, 21, and 119 days and polymer—drug miscibility (Figure 4C).

Polymer-Drug Interactions. MAS ssNMR was used to characterize two of the particle formulations, pDTy4 and pHTy7, formulated with and without dexamethasone loading. These two polymers were selected as representative samples of the extreme ends of the release rate variation across the polymers synthesized in this study, with pHTy7 releasing 99% of dexamethasone after 119 days and pDTy4 releasing only 42% in that same time. We hypothesized that if a difference in the strength of drug-polymer interactions were responsible for the difference in the release rate between these two polymers, chemical shift changes in the NMR spectra would be observed. Figure 7 compares ¹³C CP-MAS spectra of dexamethasone (Figure 7C), the empty pDTy4 particles (Figure 7A), empty pHTy7 particles (Figure 7B), and each particle loaded with dexamethasone and after 40% release. The particle formulations loaded with dexamethasone (Figure 7D and E) manifest as a linear combination of the empty polymer particle spectrum and the pure dexamethasone spectrum, with no changes in the intensity or chemical shift of the resonances observed. The lack of spectral changes indicates that both polymer-drug systems exist as a physical mixture of polymer and dexamethasone in separate phases. As seen with the miscibility parameter analysis, interactions between the polymer and the drug are not observed since the particles were prepared using a solid drug suspension. Had the drug been solubilized with the polymer during particle preparation, polymer-drug interactions might have been observed.

After 40% dexamethasone release, the phase separation for both pDTy4 and pHTy7 particles and dexamethasone is still maintained. Between the fully loaded and after 40% dexamethasone release (Figure 7F and G) the only change observed is a 40% decrease in signal intensity for resonances attributable to dexamethasone. Similar results are obtained for the ¹⁹F signal of the dexamethasone and ¹H signals of both the dexamethasone and the polymer (Figures S10, S11, and Table S4). These results indicate that the physical mixture is maintained in an aqueous environment at 37 °C and the introduction of water did not facilitate new polymer—drug interactions.

CONCLUSIONS

A thorough investigation into polymer physical and chemical properties was undertaken to understand how polymer properties affect drug release. We found that the factors that impact Fickian diffusion are sufficient to describe the drug release behavior for the polymers studied here. Additional factors that could contribute to drug release, including the affinity between the drug and the polymer matrix and changes in the segmental mobility of the polymer were not observed for this system. ssNMR data showed no interactions between the polymer and the drug investigated here, which is likely due to loading the drug as a solid suspension, and thus diffusion is controlled by the path length. This is likely the reason that the crystallite size, or the tortuosity of the diffusion path, controls the drug release rate. Larger polymer crystallite size in the bulk polymer and in the microparticles both with and without drug loading correlated with higher drug release at 7, 21, and 119 days. Additionally, we showed that particle porosity correlates to drug release as faster releasing pHTy7 particles had larger pores than the slower releasing pDTy4 particles as observed by NMR cryoporometry and SEM. Surprisingly, drug release was not related to the polymer's $T_{\rm g}$ and $T_{\rm m}$, hydrophobicity (AWCA, logP) or miscibility with dexamethasone. The correlations found between the polymer properties and drug release can aid in simplifying the design of polymers for drug delivery.

ASSOCIATED CONTENT

Supporting Information

The Supporting Information is available free of charge at https://pubs.acs.org/doi/10.1021/acsapm.1c01254.

Calculated solubility parameters, particle loading capacity, bulk polymer, empty particle, and drug-loaded particle physical and thermal properties, residual $M_{\rm n}$ retention after 119 days incubation at 37 °C, a comparison of bulk polymer $M_{\rm n}$ to cumulative drug release after 119 days, ¹⁹F and ¹H ssNMR relaxation data, dexamethasone XRD analysis, a comparison of polymer percent crystallinity and representative crystallite size for bulk polymer, empty particles, and drugloaded particles, representative profile-fitted XRD scans, kinetic modeling r^2 coefficients and profile fits, polymer–drug miscibility values, ¹⁹F and ¹H ssNMR spectra for pHTy7 and pDTy4 samples, and NMR cryoporometry calculations (PDF)

AUTHOR INFORMATION

Corresponding Author

Adam J. Gormley — Department of Biomedical Engineering, Rutgers, The State University of New Jersey, Piscataway, New Jersey 08854, United States; orcid.org/0000-0002-2884-725X; Email: adam.gormley@rutgers.edu

Authors

Catherine E. Miles — Department of Chemistry and Chemical Biology, Rutgers, The State University of New Jersey, Piscataway, New Jersey 08854, United States; orcid.org/0000-0001-7087-2689

Ashley D. Bernstein – Department of Chemistry and Chemical Biology, Rutgers, The State University of New Jersey, Piscataway, New Jersey 08854, United States

- Thomas M. Osborn Popp Department of Chemistry and Chemical Biology, Rutgers, The State University of New Jersey, Piscataway, New Jersey 08854, United States
- N. Sanjeeva Murthy Department of Chemistry and Chemical Biology, Rutgers, The State University of New Jersey, Piscataway, New Jersey 08854, United States
- Andrew J. Nieuwkoop Department of Chemistry and Chemical Biology, Rutgers, The State University of New Jersey, Piscataway, New Jersey 08854, United States; orcid.org/0000-0003-4557-1416

Complete contact information is available at: https://pubs.acs.org/10.1021/acsapm.1c01254

Author Contributions

The manuscript was written through contributions of all authors. All authors have given approval to the final version of the manuscript.

Funding

The authors acknowledge NSF CBET Award 2009942, the Rutgers University's TechAdvance program, Lubrizol Life Science, and the Nieuwkoop start-up grant from Rutgers for their help in funding this project. T.O.P. was supported by the Arnold O. Beckman Postdoctoral Fellowship in Chemical Instrumentations.

Notes

The authors declare no competing financial interest.

ACKNOWLEDGMENTS

The authors would like to thank Jarrod Cohen for providing the polymers to complete these studies and Christine Gwin for helping with microparticle preparation.

ABBREVIATIONS

API - active pharmaceutical ingredient; PLGA - poly(lactide-co-glycolide); PLLA - poly(L-lactide); HTy - 4-hydroxyphenethyl 2-(4-hydroxyphenyl)acetate; DTy - 4-hydroxyphenethyl 3-(4-hydroxyphenyl)propanoate; GPC - gel permeation chromatography; $M_{\rm n}$ - molecular weight number; HPLC - high-performance liquid chromatography; DSC - differential scanning calorimetry; $T_{\rm g}$ - glass transition temperature; $T_{\rm m}$ - melting temperature; AWCA - air—water contact angle; XRD - X-ray diffraction; ssNMR - solid state nuclear magnetic resonance; MAS - magic-angle spinning; HSK - Hoftzyer-van Krevelen.

REFERENCES

- (1) Wen, H.; Jung, H.; Li, X. Drug Delivery Approaches in Addressing Clinical Pharmacology-Related Issues: Opportunities and Challenges. *AAPS J.* **2015**, *17*, 1327–1340.
- (2) Lengyel, M.; Kállai-Szabó, N.; Antal, V.; Laki, A. J.; Antal, I. Microparticles, Microspheres, and Microcapsules for Advanced Drug Delivery. *Sci. Pharm.* **2019**, *87*, 20.
- (3) Maddali, H.; Miles, C. E.; Kohn, J.; O'Carroll, D. M. Optical Biosensors for Virus Detection: Prospects for SARS-CoV-2/COVID-19. *ChemBioChem* **2021**, 22, 1176–1189.
- (4) Sung, Y. K.; Kim, S. W. Recent Advances in Polymeric Drug Delivery Systems. *Biomater. Res.* **2020**, *24*, 1.
- (5) Patra, J. K.; Das, G.; Fraceto, L. F.; Campos, E. V. R.; Rodriguez-Torres, M. D. P.; Acosta-Torres, L. S.; Diaz-Torres, L. A.; Grillo, R.; Swamy, M. K.; Sharma, S.; Habtemariam, S.; Shin, H.-S. Nano Based Drug Delivery Systems: Recent Developments and Future Prospects. *J. Nanobiotechnol.* **2018**, *16*, 71–71.

- (6) Qi, F.; Wu, J.; Li, H.; Ma, G. Recent Research and Development of PLGA/PLA Microspheres/Nanoparticles: A Review in Scientific and Industrial Aspects. *Front. Chem. Sci. Eng.* **2019**, *13*, 14–27.
- (7) Siepmann, J.; Siepmann, F. Microparticles Used as Drug Delivery Systems. In *Smart Colloidal Materials*; Richtering, W., Ed.; Springer Berlin Heidelberg: Berlin, Heidelberg, 2006; pp 15–21.
- (8) Park, K.; Skidmore, S.; Hadar, J.; Garner, J.; Park, H.; Otte, A.; Soh, B. K.; Yoon, G.; Yu, D.; Yun, Y.; Lee, B. K.; Jiang, X.; Wang, Y. Injectable, Long-Acting PLGA Formulations: Analyzing PLGA and Understanding Microparticle Formation. *J. Cont. Rel.* **2019**, 304, 125–134
- (9) Martins, C.; Sousa, F.; Araújo, F.; Sarmento, B. Functionalizing PLGA and PLGA Derivatives for Drug Delivery and Tissue Regeneration Applications. *Adv. Healthcare Mater.* **2018**, 7, No. 1701035.
- (10) Stępień, K.; Miles, C.; McClain, A.; Wiśniewska, E.; Sobolewski, P.; Kohn, J.; Puskas, J.; Wagner, H. D.; El Fray, M. Biocopolyesters of Poly(butylene succinate) Containing Long-Chain Biobased Glycol Synthesized with Heterogeneous Titanium Dioxide Catalyst. ACS Sustainable Chem. Eng. 2019, 7, 10623–10632.
- (11) Prajapati, S. K.; Jain, A.; Jain, A.; Jain, S. Biodegradable Polymers and Constructs: A Novel Approach in Drug Delivery. *Eur. Polym. J.* **2019**, *120*, 109191.
- (12) Fredenberg, S.; Wahlgren, M.; Reslow, M.; Axelsson, A. The Mechanisms of Drug Release in Poly(lactic-co-glycolic acid)-Based Drug Delivery Systems—A Review. *Int. J. Pharm.* **2011**, *415*, 34–52.
- (13) Stewart, S. A.; Domínguez-Robles, J.; Donnelly, R. F.; Larrañeta, E. Implantable Polymeric Drug Delivery Devices: Classification, Manufacture, Materials, and Clinical Applications. *Polymer* **2018**, *10*, 1379.
- (14) Hossainy, S.; Prabhu, S. A Mathematical Model for Predicting Drug Release from a Biodurable Drug-eluting Stent Coating. *J. Biomed. Mater. Res., Part A* **2008**, *87A*, 487–493.
- (15) Macha, I. J.; Ben-Nissan, B.; Vilchevskaya, E. N.; Morozova, A. S.; Abali, B. E.; Müller, W. H.; Rickert, W. Drug Delivery From Polymer-Based Nanopharmaceuticals—An Experimental Study Complemented by Simulations of Selected Diffusion Processes. *Front. Bioeng. Biotechnol.* **2019**, *7*, 37.
- (16) Arifin, D. Y.; Lee, L. Y.; Wang, C.-H. Mathematical Modeling and Simulation of Drug Release from Microspheres: Implications to Drug Delivery Systems. *Adv. Drug Delivery Rev.* **2006**, *58*, 1274–1325.
- (17) Karavelidis, V.; Karavas, E.; Giliopoulos, D.; Papadimitriou, S.; Bikiaris, D. Evaluating the Effects of Crystallinity in New Biocompatible Polyester Nanocarriers on Drug Release Behavior. *Int. J. Nanomed.* **2011**, *6*, 3021–3032.
- (18) Feng, S.; Nie, L.; Zou, P.; Suo, J. Effects of Drug and Polymer Molecular Weight on Drug Release from PLGA-mPEG Microspheres. *J. Appl. Polym. Sci.* **2015**, *132*, 41431.
- (19) Jeong, J.-C.; Lee, J.; Cho, K. Effects of Crystalline Microstructure on Drug Release Behavior of Poly(ε -caprolactone) Microspheres. *J. Controlled Release* **2003**, 92, 249–258.
- (20) Busatto, C.; Pesoa, J.; Helbling, I.; Luna, J.; Estenoz, D. Effect of Particle Size, Polydispersity and Polymer Degradation on Progesterone Release from PLGA Microparticles: Experimental and Mathematical Modeling. *Int. J. Pharm.* **2018**, *536*, 360–369.
- (21) Wischke, C.; Neffe, A. T.; Steuer, S.; Lendlein, A. Evaluation of a Degradable Shape-memory Polymer Network as Matrix for Controlled Drug Release. *J. Controlled Release* **2009**, 138, 243–250.
- (22) Ge, J.; Neofytou, E.; Cahill, T. J.; Beygui, R. E.; Zare, R. N. Drug Release from Electric-Field-Responsive Nanoparticles. *ACS Nano* **2012**, *6*, 227–233.
- (23) Siepmann, J.; Faisant, N.; Akiki, J.; Richard, J.; Benoit, J. P. Effect of the Size of Biodegradable Microparticles on Drug Release: Experiment and Theory. *J. Controlled Release* **2004**, *96*, 123–134.
- (24) Chen, J.; Clay, N.; Kong, H. Non-Spherical Particles for Targeted Drug Delivery. *Chem. Eng. Sci.* 2015, 125, 20–24.
- (25) Zhuo, S.; Zhang, F.; Yu, J.; Zhang, X.; Yang, G.; Liu, X. pH-Sensitive Biomaterials for Drug Delivery. *Molecules* **2020**, 25, 5649.

- (26) Matsumoto, K.; Kimura, S.-I.; Itai, S.; Kondo, H.; Iwao, Y. In Vivo Temperature-sensitive Drug Release System Trigged by Cooling Using Low-melting-point Microcrystalline Wax. *J. Controlled Release* **2019**, 303, 281–288.
- (27) Cohen, J.; Shultz, R. B.; Mullaghy, A.; Gwin, C.; Kohn, J. Bioresorbable Tyrosol-Derived Poly(ester-arylate)s with Tunable Properties. *J. Polym. Sci.* **2021**, *59*, 860–869.
- (28) Cohen, J.; Bektas, C. K.; Mullaghy, A.; Perera, M. M.; Gormley, A. J.; Kohn, J. Tyrosol-Derived Biodegradable Inks with Tunable Properties for 3D Printing. *ACS Biomater. Sci. Eng.* **2021**, *7*, 4454–4462.
- (29) Bedoui, F.; Murthy, N. S.; Kohn, J. Structure and Thermal Transitions in a Biomedically Relevant Liquid Crystalline Poly(ester amide). *Macromolecules* **2017**, *50*, 2257–2266.
- (30) Patel, J. M.; Ghodbane, S. A.; Brzezinski, A.; Gatt, C. J.; Dunn, M. G. Tissue-Engineered Total Meniscus Replacement with a Fiberreinforced Scaffold in a 2-year Ovine Model. *Am. J. Sports Med.* **2018**, 46, 1844–1856.
- (31) Miles, C. E.; Gwin, C.; Zubris, K. A. V.; Gormley, A. J.; Kohn, J. Tyrosol Derived Poly(ester-arylate)s for Sustained Drug Delivery from Microparticles. *ACS Biomater. Sci. Eng.* **2021**, *7*, 2580–2591.
- (32) Gasmi, H.; Siepmann, F.; Hamoudi, M. C.; Danede, F.; Verin, J.; Willart, J. F.; Siepmann, J. Towards a Better Understanding of the Different Release Phases from PLGA Microparticles: Dexamethasone-Loaded Systems. *Int. J. Pharm.* **2016**, *514*, 189–199.
- (33) Miles, C. E.; Lima, M. R. N.; Buevich, F.; Gwin, C.; Murthy, S. N.; Kohn, J. Comprehensive Hydrolytic Degradation Study of a New Poly(ester-amide) Used for Total Meniscus Replacement. *Polym. Degrad. Stab.* **2021**, *190*, No. 109617.
- (34) Hildebrand, J. H. Solubility. J. Am. Chem. Soc. 1916, 38, 1452–1473.
- (35) Hansen, C. M. Chapter 2 Theory The Prigogine Corresponding States Theory, χ12 Interaction Parameter, and Hansen Solubility Parameters. In *Hansen Solubility Parameters: A User's Handbook*; CRC Press, Taylor & Francis Group: Boca Raton, Florida, 2007; pp 27–42.
- (36) Van Krevelen, D. W.; Te Nijenhuis, K. Chapter 7 Cohesive Properties and Solubility. In *Properties of Polymers*; Elsevier: Amsterdam, The Netherlands, 2009; pp 189–227.
- (37) Schenderlein, S.; Lück, M.; Müller, B. W. Partial Solubility Parameters of Poly(D,L-lactide-co-glycolide). *Int. J. Pharm.* **2004**, 286, 19–26
- (38) Lübtow, M. M.; Haider, M. S.; Kirsch, M.; Klisch, S.; Luxenhofer, R. Like Dissolves Like? A Comprehensive Evaluation of Partial Solubility Parameters to Predict Polymer—Drug Compatibility in Ultrahigh Drug-Loaded Polymer Micelles. *Biomacromolecules* **2019**, 20, 3041–3056.
- (39) Diversifield Enterprises (2021), Surface Tension, Hansen Solubility Parameters, Molar Volume, Enthalpy of Evaporation, and Molecular Weight of Selected Liquids. accudynetest.com/solubility_table.html (accessed May 3, 2021).
- (40) Chen, Y.; Liu, C.; Chen, Z.; Su, C.; Hageman, M.; Hussain, M.; Haskell, R.; Stefanski, K.; Qian, F. Drug—Polymer—Water Interaction and Its Implication for the Dissolution Performance of Amorphous Solid Dispersions. *Mol. Pharmaceutics* **2015**, *12*, 576–589.
- (41) Murthy, N. S.; Minor, H. General Procedure for Evaluating Amorphous Scattering and Crystallinity from X-ray Diffraction Scans of Semicrystalline Polymers. *Polymer* **1990**, *31*, 996–1002.
- (42) Morcombe, C. R.; Zilm, K. W. Chemical Shift Referencing in MAS Solid State NMR. J. Magn. Reson. 2003, 162, 479–486.
- (43) Kolodziejski, W.; Frye, J. S.; Maciel, G. E. Carbon-13 Nuclear Magnetic Resonance Spectrometry with Cross Polarization and Magic-angle Spinning for Analysis of Lodgepole Pine Wood. *Anal. Chem.* **1982**, *54*, 1419–1424.
- (44) Agrawal, A.; Rellegadla, S.; Jain, S. Chapter 4 Biomedical Applications of PLGA Particles. In *Materials for Biomedical Engineering*; Holban, A.-M.; Grumezescu, A. M., Eds.; Elsevier: 2019; pp 87–129.

- (45) Blasi, P. Poly(lactic acid)/poly(lactic-co-glycolic acid)-Based Microparticles: An Overview. J. Pharm. Invest. 2019, 49, 337–346.
- (46) Lee, B. K.; Yun, Y.; Park, K. PLA Micro- and Nano-particles. Adv. Drug Delivery Rev. 2016, 107, 176-191.
- (47) Giles, A. J.; Hutchinson, M. N. D.; Sonnemann, H. M.; Jung, J.; Fecci, P. E.; Ratnam, N. M.; Zhang, W.; Song, H.; Bailey, R.; Davis, D.; Reid, C. M.; Park, D. M.; Gilbert, M. R. Dexamethasone-Induced Immunosuppression: Mechanisms and Implications for Immunotherapy. *J. Immunother. Cancer* **2018**, *6*, 51.
- (48) Fialho, S. L.; Behar-Cohen, F.; Silva-Cunha, A. Dexamethasone-loaded Poly(ε -caprolactone) Intravitreal Implants: A Pilot Study. *Eur. J. Pharm. Biopharm.* **2008**, *68*, 637–646.
- (49) Wu, X.; Synthesis, S. Characterization, Biodegradation, and Drug Delivery Application of Biodegradable Lactic/Glycolic Acid Polymers: Part III. Drug Delivery Application. *Artif. Cells Blood Substit. Immobil. Biotechnol.* **2004**, *32*, 575–591.
- (50) Miller-Chou, B. A.; Koenig, J. L. A Review of Polymer Dissolution. *Prog. Polym. Sci.* **2003**, 28, 1223–1270.
- (51) Yarce, C. J.; Pineda, D.; Correa, C. E.; Salamanca, C. H. Relationship between Surface Properties and In Vitro Drug Release from a Compressed Matrix Containing an Amphiphilic Polymer Material. *Pharmaceuticals* **2016**, *9*, 34.
- (52) Sarmadi, M.; Behrens, A. M.; McHugh, K. J.; Contreras, H. T. M.; Tochka, Z. L.; Lu, X.; Langer, R.; Jaklenec, A. Modeling, Design, and Machine Learning-Based Framework for Optimal Injectability of Microparticle-based Drug Formulations. Sci. Adv. 2020, 6, No. eabb6594.
- (53) He, F.; Zhang, M. J.; Wang, W.; Cai, Q. W.; Su, Y. Y.; Liu, Z.; Faraj, Y.; Ju, X. J.; Xie, R.; Chu, L. Y. Designable Polymeric Microparticles from Droplet Microfluidics for Controlled Drug Release. *Adv. Mater. Technol.* **2019**, *4*, No. 1800687.
- (54) Makadia, H. K.; Siegel, S. J. Poly Lactic-co-Glycolic Acid (PLGA) as Biodegradable Controlled Drug Delivery Carrier. *Polymer* **2011**, *3*, 1377–1397.
- (55) Park, T. G. Degradation of Poly(lactic-co-glycolic acid) Microspheres: Effect of Copolymer Composition. *Biomaterials* **1995**, *16*, 1123–1130.
- (56) Arbeiter, D.; Reske, T.; Teske, M.; Bajer, D.; Senz, V.; Schmitz, K.-P.; Grabow, N.; Oschatz, S. Influence of Drug Incorporation on the Physico-Chemical Properties of Poly(l-Lactide) Implant Coating Matrices—A Systematic Study. *Polymer* **2021**, *13*, 292.
- (57) Liechty, W. B.; Kryscio, D. R.; Slaughter, B. V.; Peppas, N. A. Polymers for Drug Delivery Systems. *Annu. Rev. Chem. Biomol. Eng.* **2010**, *1*, 149–173.
- (58) Kamaly, N.; Yameen, B.; Wu, J.; Farokhzad, O. C. Degradable Controlled-Release Polymers and Polymeric Nanoparticles: Mechanisms of Controlling Drug Release. *Chem. Rev.* **2016**, *116*, 2602–2663.
- (59) Izumikawa, S.; Yoshioka, S.; Aso, Y.; Takeda, Y. Preparation of Poly(l-lactide) Microspheres of Different Crystalline Morphology and Effect of Crystalline Morphology on Drug Release Rate. *J. Controlled Release* 1991, 15, 133–140.
- (60) Petrov, O.; Furó, I.; Schuleit, M.; Domanig, R.; Plunkett, M.; Daicic, J. Pore Size Distributions of Biodegradable Polymer Microparticles in Aqueous Environments Measured by NMR Cryoporometry. *Int. J. Pharm.* **2006**, 309, 157–162.
- (61) Webber, J. B. Studies of Nano-Structured Liquids in Confined Geometries and at Surfaces. *Prog. Nucl. Magn. Reson. Spectrosc.* **2010**, 56, 78–93.
- (62) Gopinathan, N.; Yang, B.; Lowe, J. P.; Edler, K. J.; Rigby, S. P. NMR Cryoporometry Characterisation Studies of the Relation Between Drug Release Profile and Pore Structural Evolution of Polymeric Nanoparticles. *Int. J. Pharm.* **2014**, *469*, 146–158.
- (63) Permanadewi, I.; Kumoro, A. C.; Wardhani, D. H.; Aryanti, N. Modelling of Controlled Drug Release in Gastrointestinal Tract Simulation. *J. Phys.: Conf. Ser.* **2019**, *1295*, No. 012063.
- (64) Siepmann, J.; Peppas, N. A. Higuchi Equation: Derivation, Applications, Use and Misuse. *Eur. J. Pharm.* **2011**, *418*, 6–12.

- (65) Fu, Y.; Kao, W. J. Drug Release Kinetics and Transport Mechanisms of Non-degradable and Degradable Polymeric Delivery Systems. Expert Opin. Drug Delivery 2010, 7, 429–444.
- (66) Swapna, N.; Jithan, A. Preparation, Characterization and in vivo Evaluation of Parenteral Sustained Release Microsphere Formulation of Zopiclone. *J. Young Pharm.* **2010**, *2*, 223–228.
- (67) Obayemi, J. D.; Danyuo, Y.; Dozie-Nwachukwu, S.; Odusanya, O. S.; Anuku, N.; Malatesta, K.; Yu, W.; Uhrich, K. E.; Soboyejo, W. O. PLGA-Based Microparticles Loaded with Bacterial-Synthesized Prodigiosin for Anticancer Drug Release: Effects of Particle Size on Drug Release Kinetics and Cell Viability. *Mater. Sci. Eng.*, C **2016**, 66, 51–65.
- (68) Chapter 5 Mathematical Models of Drug Release. In *Strategies to Modify the Drug Release from Pharmaceutical Systems*; Bruschi, M. L., Ed.; Woodhead Publishing: 2015; pp 63–86.
- (69) Costa, P.; Sousa Lobo, J. M. Modeling and Comparison of Dissolution Profiles. Eur. J. Pharm. Sci. 2001, 13, 123–133.
- (70) Sheihet, L.; Piotrowska, K.; Dubin, R. A.; Kohn, J.; Devore, D. Effect of Tyrosine Derived Triblock Copolymer Compositions on Nanosphere Self-assembly and Drug Delivery. *Biomacromolecules* **2007**, *8*, 998–1003.